SENSITIVITY ANALYSIS OF SURFACE WIND FIELD RECONSTRUCTIONS IN TROPICAL CYCLONES

A Thesis
Presented to
The Academic Faculty

By

Emily V. Madison

In Partial Fulfillment
Of the Requirements for the Degree
Master of Science in the
School of Earth and Atmospheric Science

Georgia Institute of Technology

August, 2014

SENSITIVITY ANALYSIS OF SURFACE WIND FIELD RECONSTRUCTIONS IN TROPICAL CYCLONES

Approved by:

Dr. Dana Hartley, Advisor
School of Earth and Atmospheric Sciences
Georgia Institute of Technology

Dr. Judith A. Curry
School of Earth and Atmospheric Sciences
Georgia Institute of Technology

Dr. James Belanger
School of Earth and Atmospheric Sciences
Georgia Institute of Technology

Dr. Yi Deng
School of Earth and Atmospheric Sciences
Georgia Institute of Technology

Date Approved: June 30, 2014

DEDICATION

To my wonderful, supportive, loving parents

ACKNOWLEDGEMENTS

I wish to thank my research advisor, Dr. James Belanger, for his help in the completion of my thesis and also for his patience with me throughout this whole process. I would like to give thanks to Dr. Dana Hartley for getting me on track with and help with completing my thesis, as I needed a bit of a push near the end. I would also like to thank Dr. Judith Curry for being able to join my reading committee last minute and for her bits of encouragement and advice throughout my 2 years in the EAS department. I would like to extend a special thanks to my friends in EAS who have supported and struggled with me the past two years.

TABLE OF CONTENTS

LIST OF TABLES

LIST OF FIGURES

Page

NOMENCLATURE

AOML	Atlantic Oceanographic and Meteorological Laboratory
CFAN	Climate Forecast Applications Network
CFS-R	Climate Forecast System Reanalysis
ECMWF	European Centre for Medium-Range Weather Forecasts
GEFS	Global Ensemble Forecast System
GFS	Global Forecast System
H10	Holland 2010 hurricane radial wind model
HFIP	Hurricane Forecast Improvement Project
HRES	ECMWF High-Resolution Forecast
HUR	Hurricane
HURDAT 2	Hurricane Data generation 2
MHUR	Major Hurricane
NCEP	National Centers for Environmental Prediction
NOAA	National Oceanic and Atmospheric Administration
NON	Non-Hurricane
NWP	Numerical Weather Prediction
RMSE	Root Mean Square Error
RMW	Radius of Maximum Winds
SFMR	Stepped-Frequency Microwave Radiometer
SST	Sea Surface Temperature
TC	Tropical Cyclone

TS	Tropical Storm
VWS	Vertical Wind Shear

SUMMARY

Accurate forecasts of tropical cyclone surface wind fields are essential for decisions involving evacuation preparation and damage potential. Towards addressing these actions, a comparison of the CFAN tropical cyclone surface wind field model with the H*Wind wind field reanalyzes is done to assess the accuracy of the CFAN algorithm and to determine potential limitations of its use. 16 tropical cyclones were assessed through correlation coefficient, mean bias, and root mean square error. The resolution of initial conditions to be ingested into the model was also analyzed, along with storm type and whether or not wind shear was a limiting factor. Results suggest that the CFAN wind model accurately predicts the H*Wind analyses in most regions of the TC. The center of circulation has the highest error due to the CFAN wind model treating the center of circulation as a point rather than having finite lateral extent. Results from the sensitivity analysis based on input resolution show that the minimum input resolution for the CFAN wind model to produce fine spatial resolutions with high fidelity is 0.25°. It is shown that the reproductions of weaker tropical cyclones have lower accuracy due to wind field asymmetries within these systems, while stronger TCs are better reproduced, as these systems are usually better organized. Finally, through the wind shear analysis, it is shown that the accuracy of reconstruction is not dependent on the magnitude of vertical wind shear.

Chapter 1

Introduction

Tropical Cyclones (TC) are one of the most destructive weather phenomena in terms of both damage and lives lost. The number of people threatened by TCs has been growing, as global population and wealth have become ever more concentrated along vulnerable coastlines (Zhang and Sippel 2009; Frank and Ritchie 2001). Surface winds are highly correlated to the loss of life and damage to physical structures; surface winds also force wind waves, which affect offshore platforms and ships, and storm surge, which can exacerbate flooding, is primarily responsible for coastal inundation. Surface wind fields of TCs can be dramatically different, even when the maximum surface winds are very similar. The potential damage a given TC may cause is also related to the relative size of its wind field; where the larger the wind field, the more potential direct wind damage and potential coastal inundation (Knaff et al. 2011). Thus, the prediction of the surface wind distribution in TCs is of critical importance not only to determine intensity and potential damage from winds, but also to accurately forecast storm surge and waves, which will affect hurricane preparation and evacuation decisions. With increasing population density and coastal development, it is necessary to improve hurricane forecast models so that forecasts are more accurate at longer lead-times, so that enough advanced warning is provided for disaster preparedness and evacuation response.

There are many factors that affect prediction skill of TCs: (including but not limited to) the location where TCs generate and spend most of their lifetimes is data sparse; the quality and resolution of observational data (initial conditions), the models (e.g., numerical weather prediction (NWP) models) may not capture every process that influences a TC due to resolution, parameterizations. Furthermore, TCs themselves are part of a larger nonlinear, chaotic fluid whose characteristics are a function of atmosphere–ocean interactions. Due to this chaotic nature, there are inherent limits to the predictability timescales of TCs where the skill of the NWP model will eventually reduce to zero on timescales of a day to a week or two (Leslie et al 1998). This means that practical predictability limits must continue to be researched and improved. The limits may be with the NWP models themselves or with the observational data ingested into them.

Improvements in global dynamical and parametric models, including the forecast of tropical cyclone track and intensity have been at the forefront of tropical meteorology research. Parametric models are often used to predict TC wind fields since these have the advantage of near-zero computational cost, can be run at any desired resolution and easily can be embedded in or fully coupled to wave and storm surge models. The wind field of a TC is also functionally dependent on track and intensity, as intensity is the maximum surface wind at any location within the TC, and the location of the TC contributes to the structure and strength of the wind field especially if the TC is interacting with a surface with nonzero roughness length (e.g. topography). Accurate forecasts of track and intensity are essential to produce correct spatial distributions of the surface wind.

It is well known that TC motion is driven primarily by the large-scale environment in which it travels; motion is also influenced secondarily by structure and intensity. TC track forecasting has much improved over the last four decades with reduction in forecast errors mainly from the rapid increasing amount of observations, especially from satellites, and improvement of numerical models and assimilation schemes (Gall et al. 2013). With better initial conditions and improved modeling of the large-scale environment especially over the ocean, these enhancements can result in increased track accuracy. As previously stated, there is a natural, inherent predictability bound for every atmospheric process due to the chaotic property of the atmosphere, and it has been suggested that some global models, for example from the European Centre for Medium-Range Weather Forecasts (ECMWF), could have possibly reached the predictability limit for TC track forecasting (Plu 2011).

While track forecasting has improved significantly over the past four decades, intensity, as measured by the maximum sustained 10-m wind, forecasts has shown almost no improvement at all lead times. There are several reasons for the minimal improvement of intensity forecasts, such as: 1) intensity can be more strongly contingent upon internal dynamics and moist convection, which occur on smaller scales, is more chaotic, and less well understood, 2) the fact that the definition of intensity is an extremely local quality of a TC, and 3) because of deficiencies in the forecast models or in initial conditions that are used to produce the forecast (Zhang and Tao 2013 and Davis et al 2010). However, a recent study by DeMaria et al (2014) showed there has been a statistically significant improvement in intensity guidance between 1989 and 2012. The improvement rates for the 24-72 h forecasts were 1-2% yr^{-1} and 2-4% yr^{-1} at 96 and 120 h forecasts. The improvement rates of the 96 and 120 h forecasts were comparable to the track forecast improvement rates. These improvements were due to the transition of model guidance from climatology and persistence to statistical-dynamical and dynamical models and finally to the use of forecast consensus during the 24 yr period. Even so, the intensity forecast problem is far from solved as improvements in the warning time frame have been slowest, and skill in the prediction of rapid intensity change is still very poor. Thus, improving forecasts of CAPE, moisture through a deep layer, and the surface wind distribution should enhance intensity forecasts as genesis and intensification are highly influenced by the variations in these factors. Forecast improvement for these factors will likely come from refinement of parameterization and reductions in models horizontal grid spacing.

The severe weather community has considered at length improvement of forecast quality with increased horizontal resolution in NWP models. A higher-resolution model should be able to capture smaller-scale weather phenomena, i.e. the timing, location and structure of deep convection, more accurately. Thus, determining the impact of different resolution scales on the prediction of phenomena that involve deep, moist convection is useful. The National Oceanic and Atmospheric Administration (NOAA) has developed a 10-yr Hurricane Forecast Improvement Project (HFIP), which initially set out to determine whether greater horizontal resolution improves TC forecasts. Several groups have participated in what is referred to as the High-Resolution Hurricane test, which raised the question of whether increasing the resolution from approximately 10 km to 1-4 km produces a measurable improvement in hurricane (HUR) intensity structure prediction without degrading forecasts of position (Davis et al. 2010). There were contradictory results from these studies; some (Done et al. 2004, Kain et al. 2006, Weisman et al. 2008) suggested that increasing horizontal resolution does improve forecast quality, while others (Schwartz et al. 2009) did not. Schwartz et al.'s forecast comparisons with explicit convection at 2 km versus 4 km grid spacing did not appear to yield significant differences. Other studies echoed Schwartz et al.'s outcome that varying horizontal grid spacing between 1 and 5 km does not produce large changes in the quality of the simulation (Fierro et al. 2009), which is unexpected given that the eye wall is better resolved at higher resolutions (1 km). Davis et al. found that high-resolution forecasts performed as well as or significantly better, than coarse resolution forecasts when comparing 12-km forecasts with 4 km and 1.33 km forecasts. When comparing high-resolution forecasts, little significant difference is found, which implies that other factors may be involved in limiting the predictability of intensity forecasts.

One such factor is vertical wind shear (VWS). In general, highly sheared storms with large asymmetries generally result in poorer intensity forecasts. According to Zhang et al. (2010), the stronger the VWS, the more uncertain the intensity forecast becomes, due to rapid intensification timing differences. A negative correlation exists between VWS and TC intensity change, and it has been noted using idealized numerical models of TCs that VWS has a role in creating azimuthal asymmetries of convection. Observations of sheared TCs (magnitude of 7-15 ms^{-1}) show an influence of VWS in the storm core, where updrafts initiate downshear, maximum vertical motion in the core is downshear left and maximum precipitation is further displaced counterclockwise (Corbosiero and Molinari 2002). Tropical storm (TS) time periods appear to be affected the most as Corbosiero and Molinari (2003) showed TS time periods contain the strongest downshear signal for intensity, as (stronger) HURs should be more established to mitigate the effects of wind shear.

Even though track and intensity predictability remain on-going areas of research, understanding the predictability of the TC's wind field remains a topic that has received much less attention. Here a comparison of observational and model produced TC wind fields is analyzed to determine the accuracy of the model wind fields and its sensitivity based on input resolution. The wind fields are compared using correlation coefficients, mean bias, and root mean square error. The wind field comparisons are analyzed based on Saffir-Simpson intensity categories, initial condition input resolution, and wind shear. One of the key goals of this study is to assess the sensitivity of the wind field reconstruction process by considering how the resolution of the initial conditions impacts the reconstructions starting with finer resolution at 0.125° to coarser resolution at 1.0°. In this analysis, the wind field reconstructions with inputs of 0.125° (~10km) resolution may represent the ECMWF high-resolution (HRES). HRES's initial state is the most accurate estimate of current conditions and uses the best description of model physics and advanced data assimilation to date. The control along with the 50 lower resolution perturbed ensemble members of the ECMWF Ensemble Forecast System are represented by the 0.25° resolution reconstructions. The ensemble system provides a range of potential weather states, which provides an estimate of the uncertainty in the forecast. The Global Forecast System (GFS) is represented by the 0.5° resolution reconstructions. The GFS is produced by NCEP and is a coupled model composed of an atmospheric model, ocean model, land/soil model and sea ice model. This NWP model provides many atmospheric and land-soil variables, such as temperature, winds, precipitation, soil moisture and atmospheric ozone concentration. The final lower resolution is 1.0° is representative of other global models, such as the Global Ensemble Forecast System (GEFS). This ensemble forecast system from NCEP includes 21 total members, which also address uncertainty in initial weather observations.

To address these issues in this thesis, Chapter 2 describes the data used in analysis along with the wind field reconstruction methodology. Chapter 3 illustrates the results and the potential implications from these findings. Finally, Chapter 4 provides concluding remarks with recommendations for potential future work.

CHAPTER 2

DATA AND METHODOLOGY

2.1 Description of datasets

This research compares observations to forecasts generated by Climate Forecast Applications Network (CFAN). The observations are reanalyses from the Atlantic Oceanographic and Meteorological Laboratory (AOML) H*Wind analysis and the CFAN wind field reconstruction algorithm, temporal and surface wind speed data from the second generation Hurricane Data (HURDAT2) created by the AOML, and deep-layer vertical wind shear data from the National Centers for Environmental Prediction's (NCEP) Climate Forecast System Reanalysis (CFS-R). The CFAN wind fields are produced using initial conditions from H*Wind but at different resolutions (0.05°, 0.125°, 0.25°, 0.5°, 1.0°). Respectively, these resolutions, represent the operational CFAN wind field model, which has a similar resolution to H*Wind, the ECMWF High-Resolution, ECMWF Ensemble Leg 1, ECMWF Ensembles Leg2/GFS, and NCEP Ensembles. The varying resolutions are selected in order to assess the sensitivity of the wind field reconstruction process to the input resolution of the initial conditions.

The H*Wind analysis is an integrated TC wind analysis system which provides a dataset of the distribution of wind vectors in TCs utilizing wind measurements from multiple platforms, such as aircraft reconnaissance flight-level winds, stepped-frequency microwave radiometer (SFMR) surface wind estimates, QuikSCAT, ships, buoys, surface stations and others (Knaff et. al 2011). H*Wind analyses for 16 TCs (displayed in Table 2.1) were acquired for this study. The 16 TCs are generally Gulf of Mexico systems that affected the Florida and Gulf Coast, as the TCs occurred in regions with higher observational density giving increased confidence that the analyses are representative of the observed surface wind distribution. These 16 TCs provided 1584 unique wind fields.

Table 2.1.1 Tropical cyclones analyzed and the forecast times considered.

Storm	Time
Charley (2004)	08/13/2004 00Z - 08/14/2004 09Z
Frances (2004)	09/04/2004 06Z - 09/06/2004 12Z
Jeanne (2004)	09/24/2004 21Z - 09/26/2004 15Z
Dennis(2005)	07/08/2005 1930Z - 07/10/2005 2230Z
Katrina (2005)	08/25/2005 21Z - 08/30/2005 12Z
Rita (2005)	09/20/2005 0430Z - 09/21/2005 0430Z
Wilma (2005)	10/24/2005 1014Z - 10/24/2005 1930Z
Alberto (2006)	06/12/2006 1330Z - 06/13/2006 1630Z
Ernesto (2006)	08/29/2006 1330Z - 08/31/2006 1930Z
Barry (2007)	06/02/2007 1330Z
Fay (2008)	08/18/2008 1330Z - 08/23/2008 1930Z
Irene (2011)	08/25/2011 1330Z - 08/26/2011 2230Z
Beryl (2012)	05/27/2012 0130Z - 05/28/2012 0430Z
Debby (2012)	06/24/2012 1030Z - 06/26/2012 1930Z
Isaac (2012)	08/26/2012 0130Z - 08/29/2012 1930Z
Sandy (2012)	10/26/2012 0430Z - 10/28/2012 0130Z

The CFAN reconstruction of these 1584 wind fields requires a minimum sea level pressure value that is not supplied in the H*Wind analyses, so interpolated mean sea level pressure and corresponding time steps from HURDAT were applied. It should be mentioned that different mean sea level pressure values might have been used by AOML to generate the H*Wind analyses, which is a source of uncertainty in these comparisons. Furthermore, the reconstructed H*Wind analyses, which originally had a 3h temporal scale, were linearly interpolated to a 30 minute interval.

The CFAN horizontal 2D surface wind fields were produced at a resolution of 5 km using Holland et al. (2010), H10, 1D radial wind model based on the H*Wind wind field analyses. In order to produce the CFAN wind field reconstructions certain assumptions had to be made as some of the input data was not supplied by H*Wind. First, the environmental sea level pressure was assumed to be 1020 hPa. Next, the mean surface relative humidity along the radial direction was assumed to be 90%, and lastly, the mean sea surface temperature (SST) along the radial direction was assumed to be 28°C. These values and others which were provided by the H*Wind analysis were then used in the CFAN wind field reconstruction algorithm using the Holland 2010 hurricane radial wind model (Holland et al. 2010) to produce 1D surface winds.

H10 first calculates the radial surface pressure profile using a modified rectangular hyperbola:

$$p_s = p_{cs} + \Delta p_s e^{-\left(\frac{r_{vm}}{r}\right)^b},$$

where p_s is the surface pressure at radius r, p_{cs} is the central pressure, $\Delta p_s = p_{ns} - p_{cs}$ is the pressure drop from a defined external pressure p_{ns} to the cyclone center, and *b* is a scaling parameter that defines the proportion of the pressure gradient near the radius of maximum winds r_{vm}. The subscript m denotes maximum. Next, the surface wind v_s is assessed using

$$v_s = \left[\frac{100 b_s \Delta p_s \left(\frac{r_{vms}}{r}\right)^{b_s}}{\rho_s e^{\left(\frac{r_{vm}}{r}\right)^{b_s}}}\right]^x$$

where the subscript s signifies surface values at a nominal height of 10m and ρ_s is the air density at the surface. The exponent x varies linearly as such:

$$x = 0.5 \qquad\qquad\qquad r \leq r_{v_m},$$

$$x = 0.5 + (r - r_{v_m})\frac{x_n - 0.5}{r_n - r_{v_m}} \quad r > r_{v_m},$$

where x_n is the adjusted exponent to fit the peripheral observations at a defined radius r_n. Here, b_s is kept constant and is related to the original b such that $b_s = bg_s^x$ where g_s is the reduction factor for gradient-to-surface winds. In order to determine the surface wind v_s the following data is required: the central pressure, radius of maximum winds, an external pressure and collocated surface wind speed, and surface air density. The parameter b_s can be derived using:

$$b_s = \frac{v_{ms}^2 \rho_{ms} e}{100(p_{ns} - p_{cs})},$$

if v_{ms} and the central pressure have been directly measured.

A good estimate of the surface air density can be determined as follows:

$$\rho_s = \frac{100 p_s}{R T_{vs}},$$

$$T_{vs} = (T_s + 273.15)(1 + 0.61 q_s),$$

$$q_s = RH_s\left(\frac{3.802}{100 p_s}\right) e^{\frac{17.67 T_s}{243.5 + T_s}}, \quad \text{and}$$

$$T_s = SST - 1.$$

The gas constant for dry air R is 286.9 J kg^{-1} K^{-1}, T_{vs} is the virtual surface temperature in K, T_s is the surface temperature in °C, q_s is the surface moisture in g kg^{-1}, RH_s is the surface relative humidity, and SST is the sea surface temperature. The assumed values for RH_s and SST were stated earlier.

To generate 2D surface wind distributions, these 1D fields were calculated at a one degree angular rate of change spanning a 90 degree window centered on the angle in order to assess maximum winds, the radius of maximum winds (RMW), outer wind speed and the radius of outer winds. The output surface wind value assigned was determined by the Holland wind field and associated distance found using the radial distance spacing between the grid cells and the TC center. A Monte Carlo resampling approach was used to vary the outer wind speed threshold, which improved the robustness of the reconstruction. The outer wind speed threshold was allowed to vary between 25% and 75% of the max 10 m wind speed per specified quadrant. Finalized output grid cell wind speed represents the average of 90 separate 1D wind field fits. In order to agree with standard open land exposure adjustment values, wind speeds over land were reduced by 17% as suggested by Vickery (2007). To conduct the sensitivity analysis, this reconstruction process was replicated to produce high-resolutions surface wind fields, except varying the input resolution of the initial H*Wind data.

HURDAT2 is the official TC tracking dataset for the North Atlantic and consists of tropical cyclone 6-hourly positions and maximum wind speed estimates and is updated annually by the National Hurricane Center (Neumann et al. 1999). The 6-hourly time steps and their corresponding maximum 1-minute sustained wind speeds at 10 meters for each storm were acquired from HURDAT2. These values were linearly interpolated to obtain a half-hourly time scale and the wind speeds at each half-hour. The half-hourly maximum wind speed information was then used to separate the H*Wind and CFAN wind fields into (NON) tropical storm files (maximum wind < 64 kts), (HUR) hurricane files (maximum wind ≥ 64 kts) and (MHUR) major hurricane files (maximum wind ≥ 96 kts).

CFS-R data was used to obtain hourly vertical deep layer (850-200 hPa) wind shear during the time periods of the 16 TCs. The CFS-R is a global, high-resolution, coupled atmosphere-ocean-land surface-sea ice model providing the best estimate of the state of these coupled domains over the period of 1979 to 2010 (Saha et al. 2010). The current CFS-R is extended as an operational, real time product. The global atmospheric resolution is ~38 km with 64 levels extending from the surface to 0.26 hPa. The CFS-R atmospheric products are available at an hourly time resolution and 0.5° horizontal resolution. The average wind shear was calculated over a 500 km distance from the TC center using the location of the TC center as determined by HURDAT 2 using the following equation:

$$shear = \sqrt{\overline{(U_{850}} - \overline{U_{200})}^2 - \overline{(V_{850}} - \overline{V_{200})}^2}$$

, where U and V the zonal and meridional winds at all points within 500 km of the center, the subscript is the level of the atmosphere at which the wind is measure in hPa, and the over bar represents the mean of the winds within 500 km of the center at each level. The location of the TC center is likely to differ somewhat from where the TC is centered in the CFS-R. However, since the calculation occurs over a 500 km radius, small differences in the center location are likely to have minimal impact to the shear magnitude. The vertical deep layer wind shear and concurring dates were interpolated to a half-hourly time scale to facilitate comparison.

Since the distribution of vertical wind shear is non-normal (Figure 2.1.1), the median of the vertical wind shear distribution was found in order to classify TCs embedded with high wind shear and low wind shear environments. This value was 6.2525 ms^{-1}, so low shear ≤ 6.2525 ms^{-1} and high shear > 6.2525 ms^{-1} were determined as such. The times where the TC was experiencing low or high shear were used to partition the H*Wind and CFAN wind field files into low and high shear bins. Furthermore, the wind fields were rotated about the storm center so that the wind shear vector was pointing north. This is done in order to evaluate the effect of vertical wind shear on the TC wind fields, given that vertical wind shear induces known asymmetries in the precipitation distribution and surface wind field.

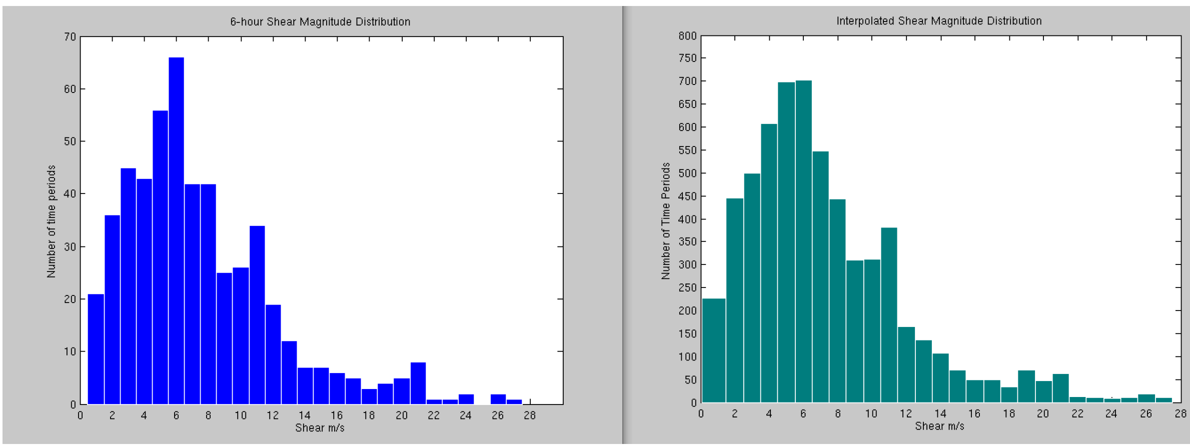

Figure 2.1.1. Distribution of 6-hour (left) and interpolated (right) deep-layer VWS in the 1584 wind fields analyzed with shear magnitude on the x-axis and number of time periods on the y-axis. Shows right skewness meaning TCs are unable to sustain themselves in environments where vertical wind shear is strong.

2.2 H*WIND and CFAN Comparison Methodology

The CFAN's surface wind field reconstructions are evaluated relative to the H*Wind analyses using correlation, mean bias and root mean square error. These three statistical methods were implemented on all TC dates, TC dates separated by maximum wind speed (tropical storm, hurricane, major hurricane), all TC dates at different spatial resolutions, and those dates where a TC experienced low and high wind shear. The 2D wind fields have to be normalized by a common metri, so that the TCs characteristic structure may be compared with one another, as tropical cyclones have varying sizes. The normalization in this case was with respect to the radius of maximum winds such that distances from the TC center are recast in normalized units of RMW-relative distance.

To measure the skill or quality of the CFAN reconstructions, the correlation between the CFAN reconstructions and the H*Wind reconstructions is calculated. The correlation coefficient, *r*, measures the strength and indicates the direction of the linear association between two variables (e.g. model output and observed values). The Pearson product-moment correlation coefficient is the method of correlation used, which is obtained by dividing the covariance of the two variables by the product of their standard deviations.

$$r = \frac{\sum_{i=1}^{n}(x_i-\bar{x})(y_i-\bar{y})}{\sqrt{\sum_{i=1}^{n}(x_i-\bar{x})^2 \times \sum_{i=1}^{n}(y_i-\bar{y})^2}}.$$

The correlation is +1 in the case of a perfectly increasing linear relationship, and -1 in the case of a perfectly inverse linear relationship, with the values in between indicating the degree of linear relationship. A correlation of zero means there is no linear relationship between the variables.

In order to determine the amount of variance the CFAN reconstructions explain in H*Wind for the shear cases, the r-squared value was determined for the points outside 0.5 RMW and within 0.25 RMW. The coefficient of determination, r^2, gives the proportion of the variance of one variable that is predictable from the other variable, or the ratio of the explained variation to the total variation. The coefficient of determination is such that $0 \leq r^2 \leq 1$, and denotes the strength of the linear association between two variables. The higher the r-squared value, the better the model fits the observed data.

The statistical significance of the correlation values for TCs by intensity and resolution was determined using the two-tailed student's t-test with the null hypothesis that the correlations are due simply to random chance alone. One needs to determine the t-distribution of the data and the critical t-value based on the degrees of freedom and the confidence. If the t-distribution value is greater than the critical t-value, then one can reject the null hypothesis, which implies that the correlation values have statistical significance at the chosen confidence level.

Another method of determining statistical significance of a correlation is using the percentile method of bootstrap resampling. It is often used as a non-parametric alternative to inferences based on parametric assumptions (e.g. the outcome is normally distributed) when those assumptions are in doubt. Bootstrap resampling is generally more stringent and robust and is often used when the sample size is small or non-Gaussian. This method is used to determine the statistical significance of the reconstructed wind fields for high and low wind shear cases. The bootstrap procedure involves choosing random samples with replacement (Monte Carlo resampling) from a data set, e.g. H*Wind and CFAN wind field reconstructions composites, and analyzing each sample the same way creating a large number of bootstrap samples (1000 or more) at a certain confidence level. Sampling with replacement means that each observation is selected separately at random from the original dataset; so a particular data point from the original data set could appear multiple times in a given bootstrap sample. The number of elements in each bootstrap sample equals the number of elements in the original data set. The correlation is considered significant if the lower bound (2.5%) of the correlation is greater than 0, i.e. if a correlation is significantly different from 0 at the 0.05 level, then the 95% confidence interval will not contain 0. Whenever an effect is significant, all values in the confidence interval will be on the same side of zero, either all positive or all negative.

Mean bias and root mean square error are used to measure the accuracy of the CFAN reconstructions. The mean bias is simply the average difference between two variables, in this case the H*Wind and CFAN reconstructions. $MB = \overline{f - a}$, where f is the forecast values and a is the observed values. It is used to determine forecast error. When the value is positive, the model has an over-forecast bias, and when the value is negative, the model has an under-forecast bias.

The root mean square error (RMSE) measures the distance between the forecast and verifying analysis, or observations, i.e. $RMSE = \sqrt{\overline{f - a}^{\,2}}$. It is a measure of the typical spread of the data around the regression line. It is negatively oriented meaning increasing numerical values indicate increasing failure and is directly interpretable in terms of measurement units, as it has the same units as the forecast variable that is analyzed.

CHAPTER 3

RESULTS AND DISCUSSION

The correlation coefficient, mean bias and root mean square error between the H*Wind and CFAN surface wind fields from 2004–2012 were calculated, for all wind fields at different initial resolutions, for NON (max wind speed < 64kts), HUR (max windspeed > 64 kts) and MHUR (max wind speed ≥ 96 kts) wind fields, and tropical cyclones that experienced low wind shear and high wind shear. The unique wind fields in each analysis are detailed in Table 3.1. The large sample size of wind fields allowed for robust statistical evaluation.

Table 3.1. The number of unique windfields in each analysis. ‘All’ includes the initial H*Wind versus CFAN analysis and the analyses at different resolutions.

Analysis	**Number of Wind Fields**
All	1584
Non-hurricane	817
Hurricane	763
Major Hurricane	281
Low Shear	804
High Shear	742

Counts a few hundred or so prove important for maintaining robust statistics in the analyses (Davis et al. 2010). The statistical significance of the correlation coefficient was tested at the 99% confidence level using the t-test for all wind fields, for wind fields at differing resolutions and wind fields for each TC type. A bootstrap resampling test was used to evaluate the significance of the wind shear surface wind fields. Nearly all wind field comparison correlations were statistically significant at 99% (MHUR has a small section which is not statistically significant at 99%).

The correlation coefficient in RMW relative distances for all wind fields from 2004–2012 is shown in Figure 3.1a. For all locations outside 0.5 RMW, the CFAN wind fields reproduce on average 95% of the total variance of H*Wind, while within 0.25 RMW 28% of the total variance of H*Wind is explained by the CFAN model. The CFAN model does an excellent job at reconstructing nearly all of the variability in the H*Wind analyses for most locations within a TC according to these findings (e.g. locations outside 0.5 RMW relative distance).

Further insight into the structural biases of the surface reconstructions is provided in Figures 3.1b, which displays the mean bias (CFAN –H*Wind; in knots (kts)) for all surface wind fields. The maximum bias (12.5 kts) is found at an RMW relative distance of 0.20 in the left-rear quadrant; this bias is approximately twice the observational uncertainty of the surface wind measurements, which is ± 5 kts. At the RMW, the mean bias is 3.4 kts. The largest positive biases occurring within 0.5 RMW relative distance suggests a deficiency in the CFAN model for correctly estimating the lateral extent of the TC's center of circulation, or eye, which is also supported by the findings from the RMSE (in kts) in Figure 3.1c. The largest RMSE is found within 0.5 RMW distance at 15.5 kts.

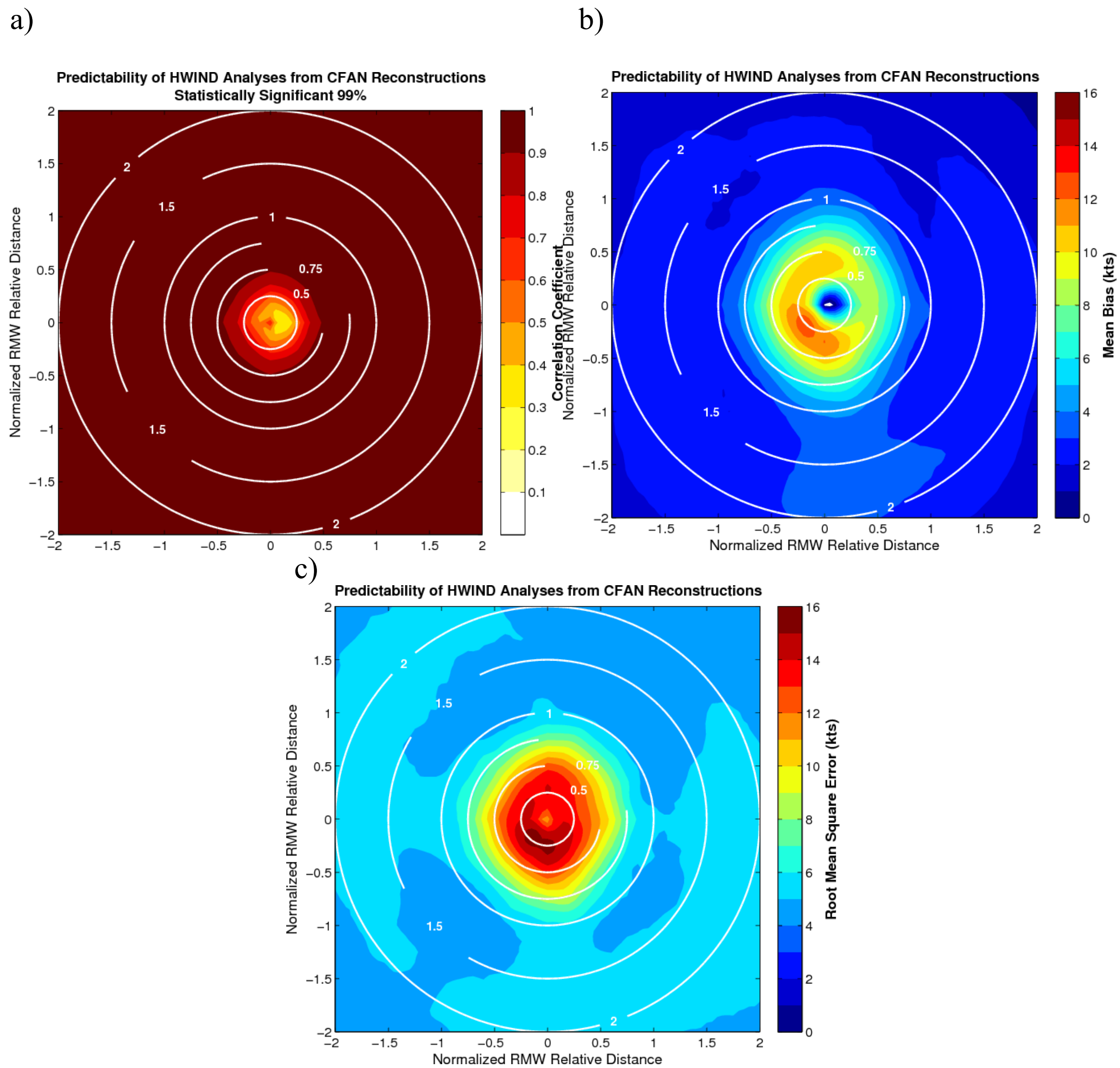

Figure 3.1: a) Correlation coefficients (shaded) between CFAN wind field reconstructions and H*Wind analyses in radius of maximum winds relative distances. b) Similar to a), except for mean bias in kts (shaded). Positive biases indicate CFAN wind values are larger than H*Wind. c) Similar to a) and b), except for RMSE in kts (shaded). White concentric circles show RMW relative distances at normalized intervals of 0.25, 0.5, 0.75, 1, 1.5, and 2.

These results are consistent with the current configuration of the CFAN wind field model. In the current version, the TC's center of circulation is treated as a point, when in reality it has finite lateral extent. One then would expect for TCs that possess an eye of small horizontal size, the mean biases and errors are likely to occupy smaller horizontal area, while TCs with larger eyes, the radial wind speeds within the center of circulation are likely to be overestimated on average by 5–10 kts. Even with this minor deficiency, the CFAN wind field model provides an excellent reproduction of the H*Wind analyses outside of the center of circulation, which suggest that the wind field reconstruction process is not a predictability-limiting factor.

The next analysis determines the resolution(s) of the initial conditions which are proficient enough at reproducing the H*Wind surface wind fields with high fidelity. Higher resolution models generally have longer processing times than lower resolutions models, so the efficiency of the reproduction process can be improved if a lower resolution model that sufficiently reproduces the surface wind fields can be used. A threshold for horizontal resolution is determined by examining the correlation coefficient, mean bias, and RMSE of all 1584 wind fields at different initial input resolutions (0.125^{o}, 0.25^{o}, 0.5^{o}, 1.0^{o}). These different resolutions are compared to the initial analysis, which has an input resolution of 0.05^{o}, as the CFAN wind fields with this input resolution explained the majority of the variability in the H*Wind wind fields.

Figure 3.2a shows the correlation coefficient for all wind fields from 2004–2012 using initial conditions at an input resolution of 0.125^{o}. The average total variance explained outside of 0.5 RMW relative distance is 92%, which is slightly less than the average total variance explained in the same area of the wind fields at 0.05^{o}. The average total variance (26%) within 0.25 RMW is also similar to that found in the 0.05° degree correlation coefficient analysis. The 0.125° resolution CFAN wind fields still explain a large majority of the H*Wind wind fields suggesting that a reconstruction based on a model with 0.125° input resolution also does an excellent job of reproducing the H*Wind surface wind fields outside of 0.5 RMW relative distance.

The mean bias shown in Figure 3.2b has a max bias of 12.4 kts at a distance of 0.21 RMW in the rear-left quadrant, which is nearly the same magnitude and location as the max bias in the 0.05 degree resolution mean bias. The average bias at the RMW is 1.3 kts, which is 2 kts less than the 0.05 degree average bias at this distance. The RMSE in Figure 3.2c has a max RMSE (16 kts) within 0.5 RMW, again similar to that in the 0.05° analysis. The model deficiency of defining the lateral extent of the center of circulation of a TC is reinforced here as the max biases and errors occur within a 0.5 RMW relative distance.

The correlation coefficient of the 1584 wind fields with 0.25° resolution initial conditions is displayed in Figure 3.3a. The average total variance outside of 0.5 RMW (82%) is over 10% lower than that at 0.05° resolution. The surface wind within 0.25 RMW is still difficult to resolve due to the lack of definition of the lateral extent of the eye, but a degradation in the accuracy of the wind field reproduction is apparent outside of this area at 0.25° resolution.

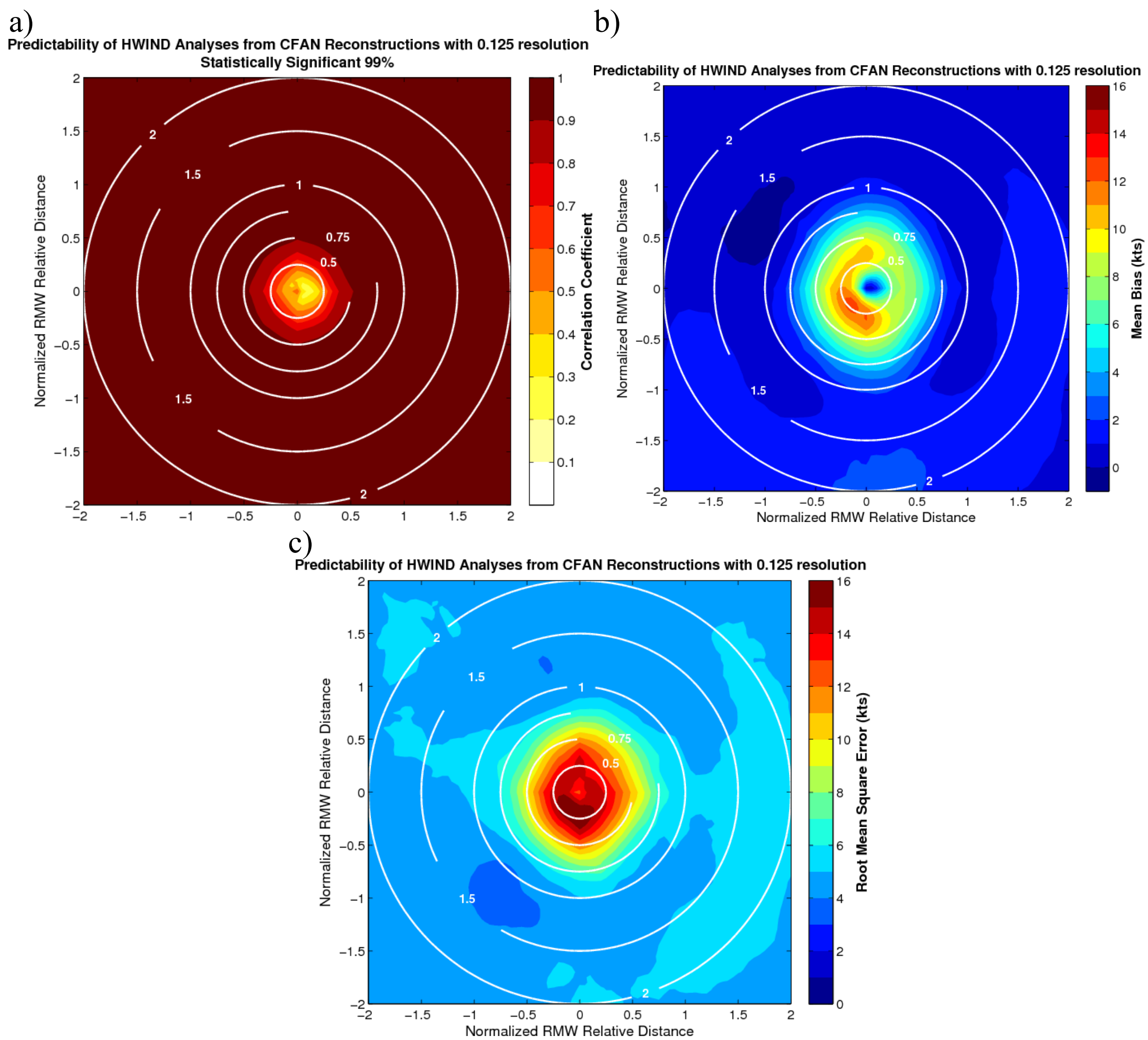

Figure 3.2: a) Correlation coefficients (shaded) between CFAN wind field reconstructions at 0.125° resolution and H*Wind analyses in radius of maximum winds relative distances. b) Similar to a), except for mean bias in kts (shaded). Positive biases indicate CFAN wind values are larger than H*Wind. c) Similar to a) and b), except for RMSE in kts (shaded). White concentric circles show RMW relative distances at normalized intervals of 0.25, 0.5, 0.75, 1, 1.5, and 2.

In Figure 3.3b the mean bias (0.25° CFAN – H*Wind; in kts) is shown. The max bias is similar in magnitude and found at a the same RMW distance and location as the max bias in the precious two resolutions, but now the bias at the RMW is negative, meaning the radial winds in this area are under-predicted. The structure outside of 1 RMW for the 0.25° resolution mean bias is different than that of 0.05° resolution mean bias, as there are areas where the bias exceeds -5 kts, while in the 0.05° mean bias analysis, errors are below 2 kts outside 1 RMW. This is further supported in the RMSE of the 0.25° resolution wind fields (Figure 3.3c) as the RMSE has increased outside of the RMW.

In Figure 3.4a the correlation coefficient based on input surface winds at 0.5^{o} resolution is shown. The average total variance outside of 0.5 RMW relative distance (72%) considerably decreased, as compared to the average total variance outside of 0.5 RMW in the 0.05° resolution analysis.

Figure 3.4b shows the mean bias for the 0.5° resolution wind fields. The biases are larger overall for these wind fields as compared to the higher resolution wind fields. They are mostly underforecasted between -3 to -7 kts, but with areas closer to -10kts outside of 0.75 RMW. The RMSE has also increased (Figure 3.4c) where the RMSE at the RMW is nearly 10 kts greater than that of the 0.05° and 0.125° resolution RMSEs. The RMSE is also greater than 7 kts in the 2 RMW by 2 RMW area of the wind field.

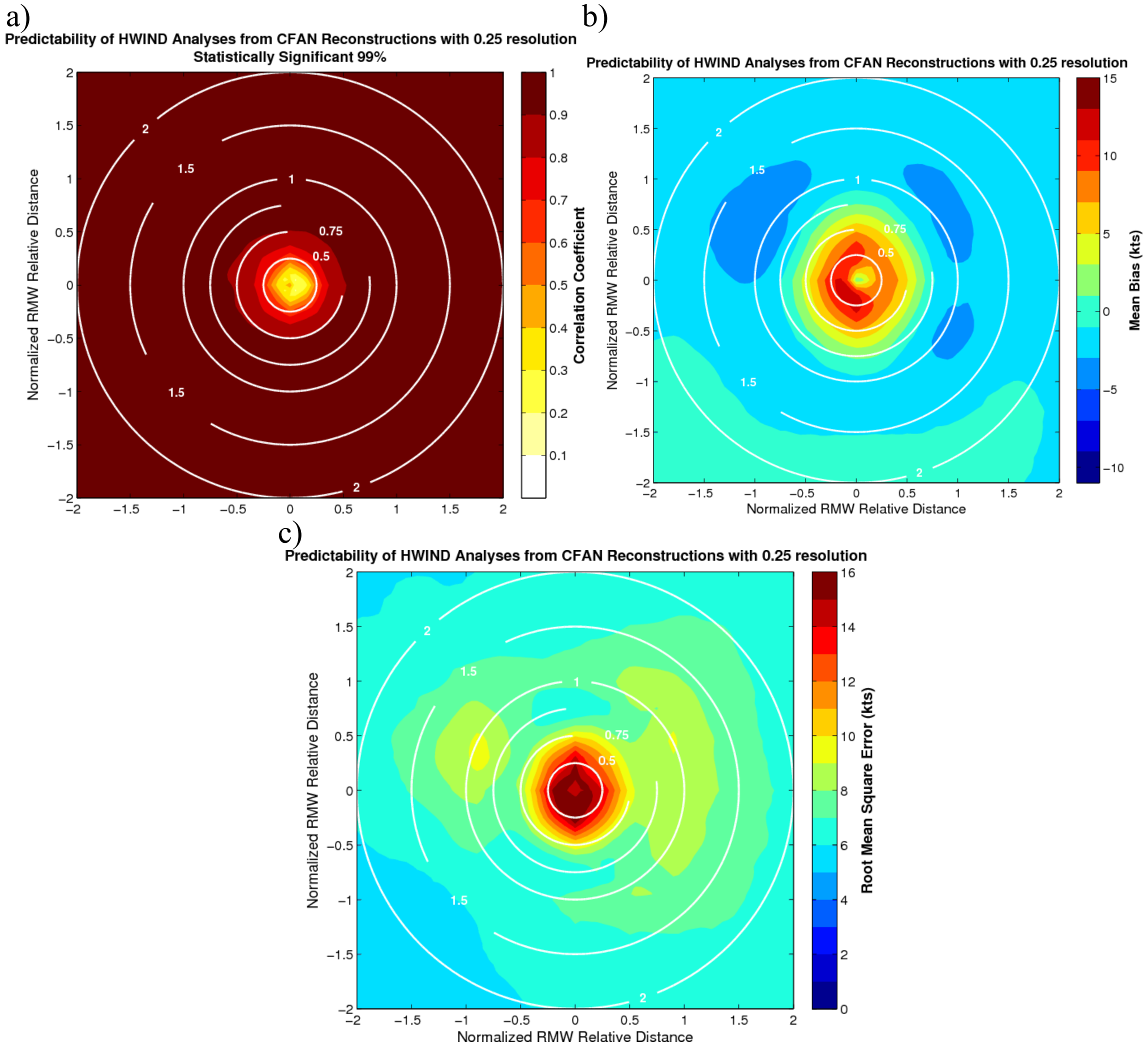

Figure 3.3: a) Correlation coefficients (shaded) between CFAN wind field reconstructions at 0.25° resolution and H*Wind analyses in radius of maximum winds relative distances. b) Similar to a), except for mean bias in kts (shaded). Positive biases indicate CFAN wind values are larger than H*Wind. c) Similar to a) and b), except for RMSE in kts (shaded). White concentric circles show RMW relative distances at normalized intervals of 0.25, 0.5, 0.75, 1, 1.5, and 2.

The correlation coefficient of the 1.0 ° resolution wind fields is shown in Figure 3.5a. A significant decrease in the average total variance explained outside 0.5 RMW (53%) occurred in the 1.0 degree resolution correlation coefficient. Figure 3.5b shows the mean bias for this resolution, which displays large biases in the area where surface wind should be well forecasted (e.g. outside 0.5RMW). The RMSE for the 1.0 degree resolution windfields (Figure 3.5c) also supports the poor forecast skill with the max RMSE at 23.9 kts at 1.03 RMW.

The results of the wind field resolution analyses show that the 0.5° and 1.0° wind fields have a tendency to strongly underrepresent the observed winds by 15–25kts, which is symptom of lower resolution models.

In Figure 3.6 the wind profiles of RMW relative distance versus mean wind speed for each resolution are shown as another means to visualize the differences in wind speeds for each resolution. There is a significant decrease in the maximum wind speed in general with 0.5 and 1.0 degree input resolution profiles, which was seen in the 2D surface wind field analyses. The 0.05 and 0.125 maximum wind speed share only approximately a 5 kt difference at the RMW, but follow a similar profile outside of this area. The lower the resolution the larger the mean wind speed at 0 RMW, or the center of circulation. This feature is important as the center of circulation should have a smaller wind speed overall.

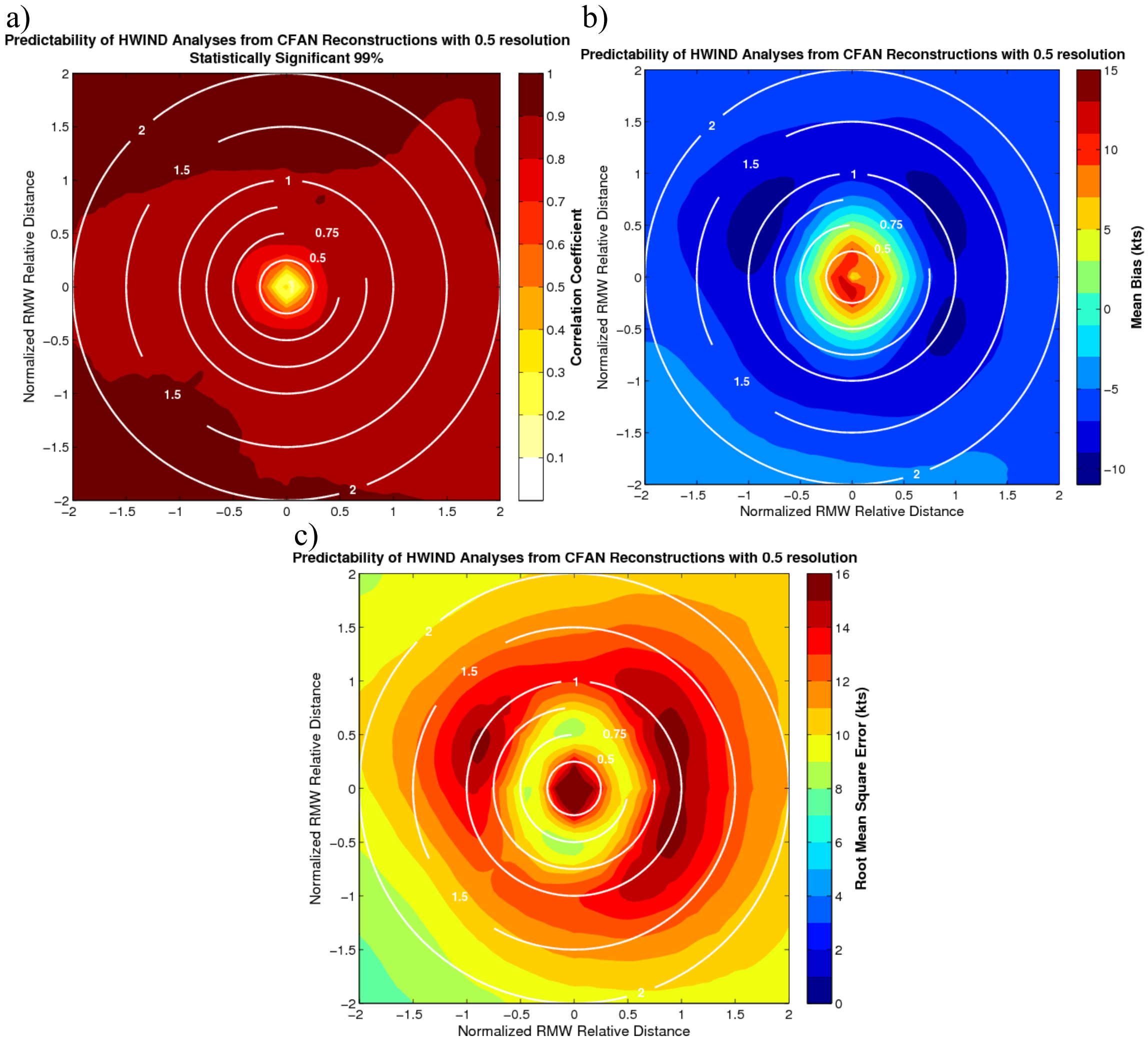

Figure 3.4: a) Correlation coefficients (shaded) between CFAN wind field reconstructions at 0.5° resolution and H*Wind analyses in radius of maximum winds relative distances. b) Similar to a), except for mean bias in kts (shaded). Positive biases indicate CFAN wind values are larger than H*Wind. c) Similar to a) and b), except for RMSE in kts (shaded). White concentric circles show RMW relative distances at normalized intervals of 0.25, 0.5, 0.75, 1, 1.5, and 2.

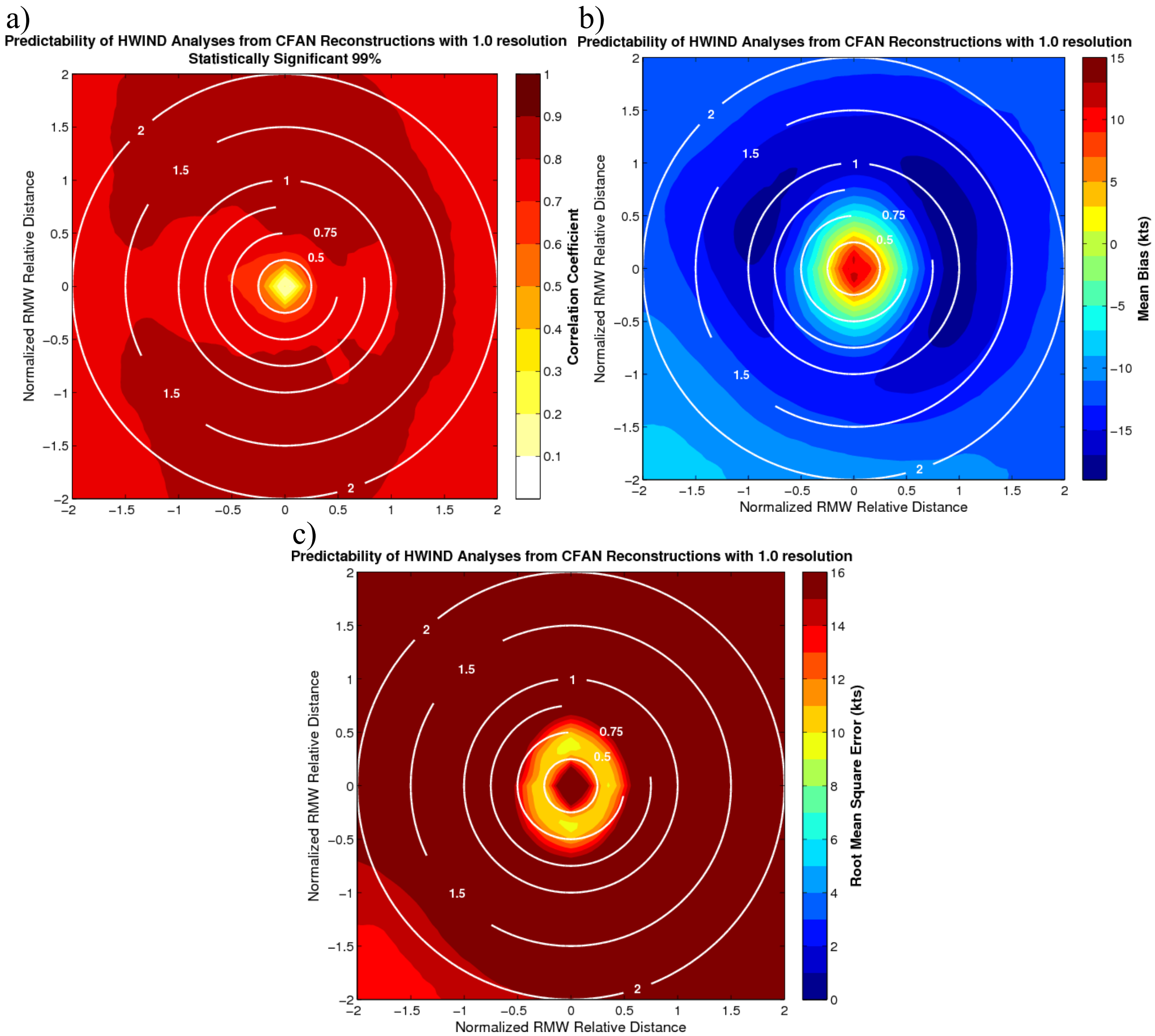

Figure 3.5: a) Correlation coefficients (shaded) between CFAN wind field reconstructions at 1.0° resolution and H*Wind analyses in radius of maximum winds relative distances. b) Similar to a), except for mean bias in kts (shaded). Positive biases indicate CFAN wind values are larger than H*Wind. c) Similar to a) and b), except for RMSE in kts (shaded). White concentric circles show RMW relative distances at normalized intervals of 0.25, 0.5, 0.75, 1, 1.5, and 2.

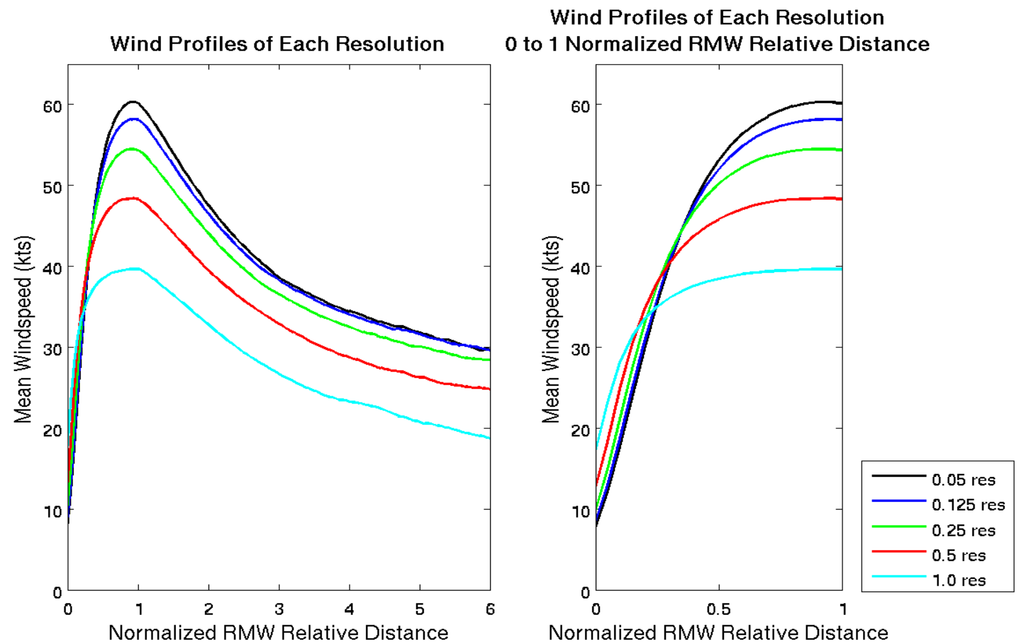

Figure 3.6. Left Panel shows the wind profiles of each resolution with normalized RMW relative distance versus (0-6 RMW) mean wind speed (kts). The right panel is similar to left panel except that it is zoomed in to RMW between 0 – 1.

Overall 0.125° resolution wind fields show a relatively small difference from 0.05° resolution wind fields, so using 0.125° resolution model for initial conditions is viable. The 0.25° resolution wind fields have slightly larger differences, but may be usable if a bias-adjustment is made. The 0.5° and 1.0° resolution models should be avoided if possible for initial conditions, as the grid spacing is just too large to resolve the maximum wind speed and location of maximum winds, which is detrimental to determining the distribution of the wind field profile.

The next analysis separates the wind fields into NON, HUR, and MHUR categories with the input resolution of 0.05° in order to assess how well the model reproduces surface winds for different TC types and further ascertain potential sensitivities in the wind field algorithm.

The nonhurricane correlation coefficient in Figure 3.7a has an average total variance outside 0.5 RMW of 89%, and within 0.25RMW the average total variance is 16%. The mean bias in Figure 3.7b shows a max bias of 11.1 at 0.3 RMW relative distance and a bias of 3 kts at the RMW. The max RMSE in Figure 3.7c is 13.7 kts at 0.18 RMW and the RMSE at the RMW is 4.8 kts.

Figure 3.8a shows the HUR case has a more compact area of correlation coefficient that is less than 1, which does not reach 0.75 RMW, than that of the NON case. It is also more concentric due to stronger TCs being more symmetric than weaker TCs. The variance explained within 0.25 RMW is the same as the NON; however, the variance outside of 0.5 RMW is 93%. The max bias in the mean bias analysis of HUR (Figure 3.8b) is 14.6 kts at a distance of 0.28 RMW, with the bias at the RMW of 3.8 kts. The max RMSE in the RMSE figure for HUR (Figure 3.8c) is 17.4 kts at 0.25 RMW and at the RMW the RMSE is 6.2 kts.

The MHUR correlation coefficient is displayed in Figure 3.9a. The average total variance outside 0.5 RMW relative distance is 93%, which is the same as the HUR average total variance in this area. The mean bias of the MHUR wind fields shown in Figure 3.9b has a max bias of 18.3 kts at 0.28 RMW. The MHUR wind fields have higher biases between 0.75 RMW and the center than NON and HUR with HUR and MHUR having slightly larger biases overall compared to NON.

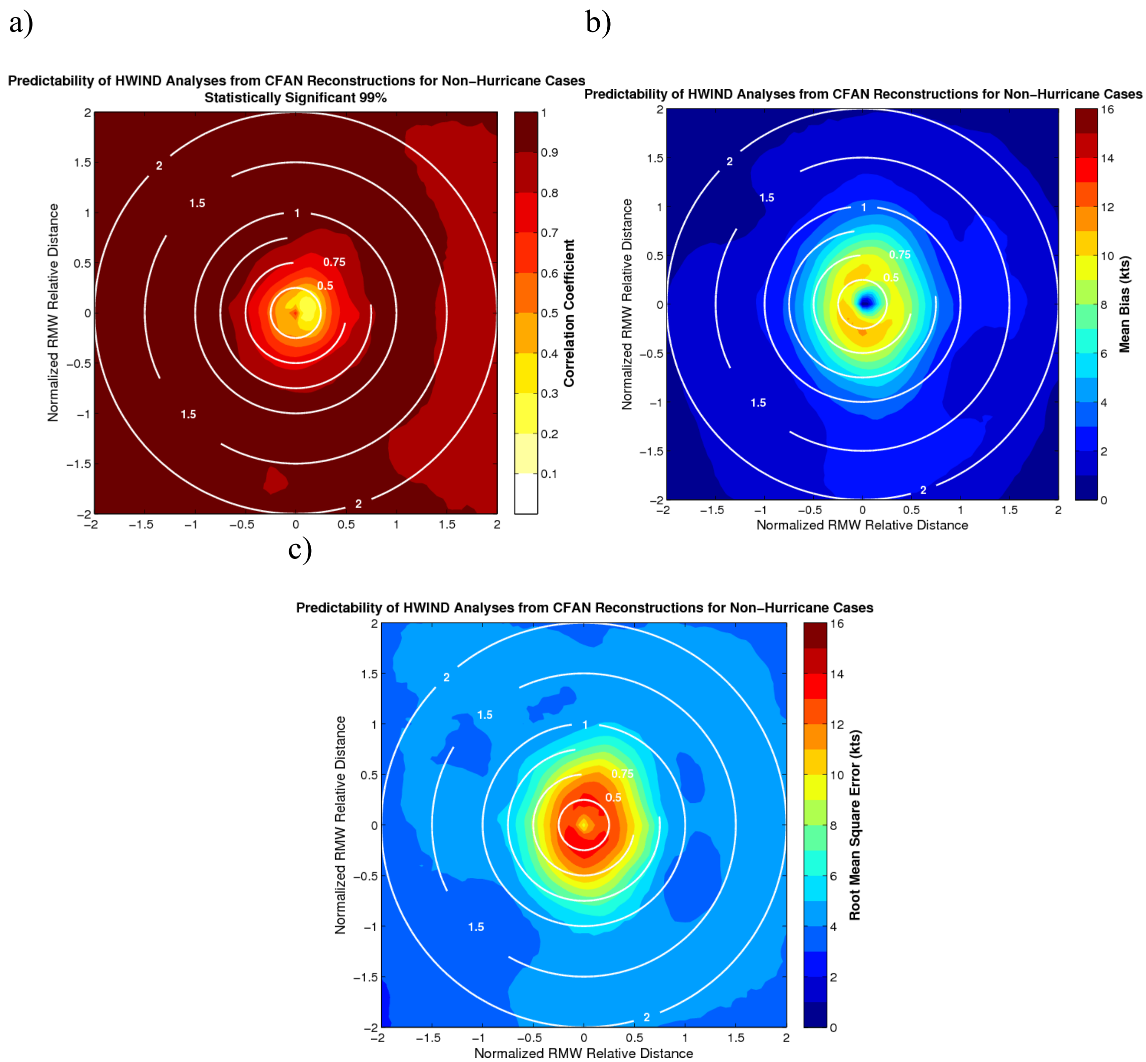

Figure 3.7: a) Correlation coefficients (shaded) between non-hurricane CFAN wind field reconstructions and H*Wind analyses in radius of maximum winds relative distances. b) Similar to a), except for mean bias in kts (shaded). Positive biases indicate CFAN wind values are larger than H*Wind. c) Similar to a) and b), except for RMSE in kts (shaded). White concentric circles show RMW relative distances at normalized intervals of 0.25, 0.5, 0.75, 1, 1.5, and 2.

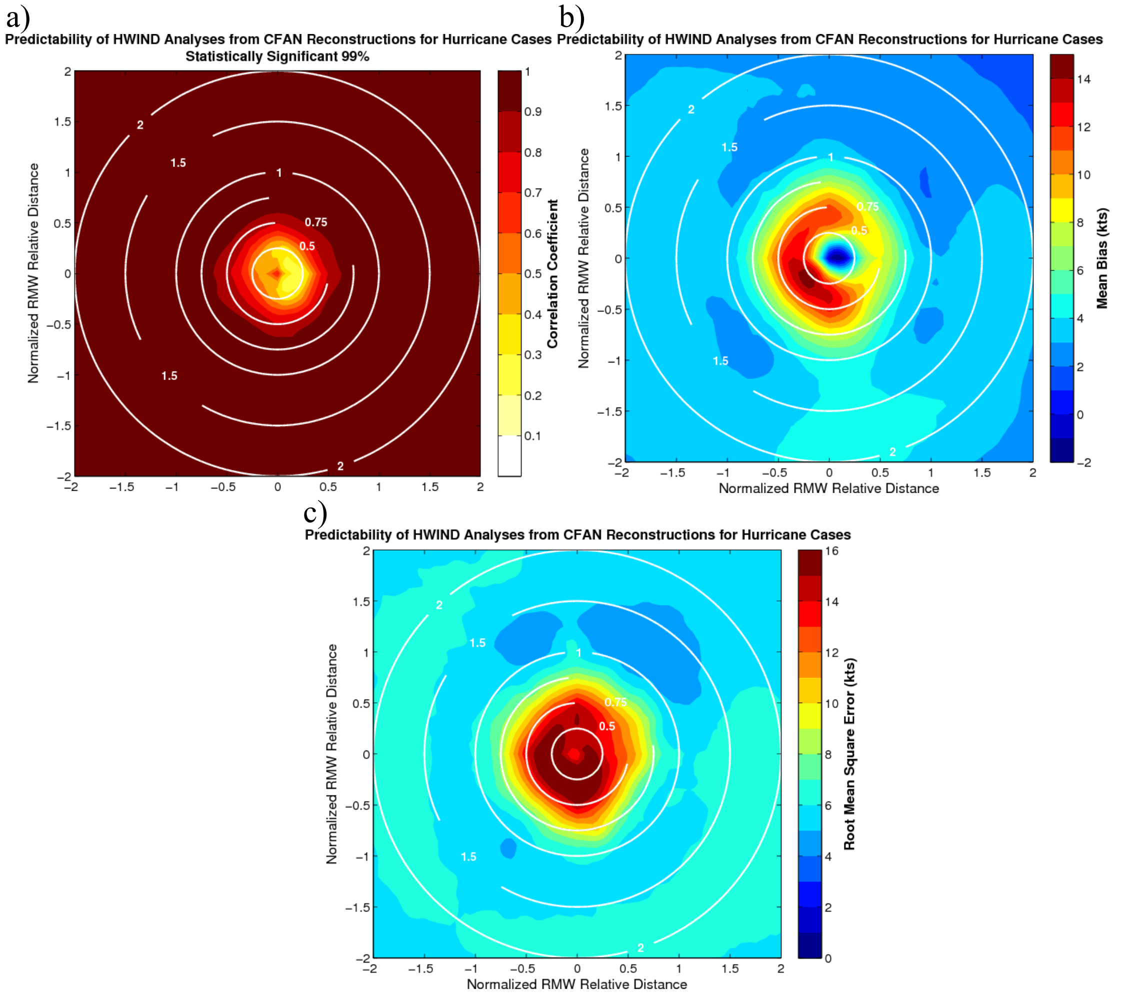

Figure 3.8: a) Correlation coefficients (shaded) between hurricane CFAN wind field reconstructions and H*Wind analyses in radius of maximum winds relative distances. b) Similar to a), expect for mean bias in kts (shaded). Positive biases indicate CFAN wind values are larger than H*Wind. c) Similar to a) and b), except for RMSE in kts (shaded). White concentric circles show RMW relative distances at normalized intervals of 0.25, 0.5, 0.75, 1, 1.5, and 2.

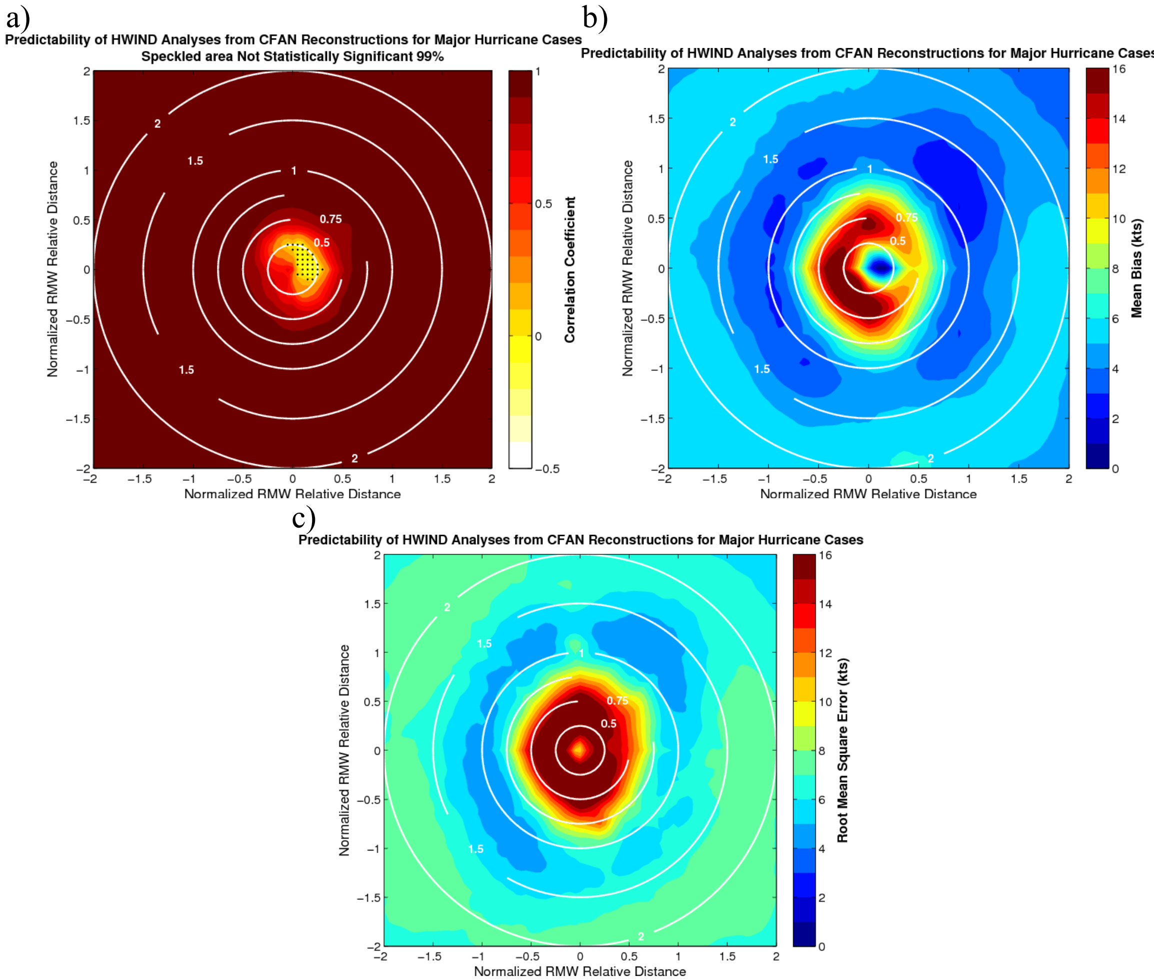

Figure 3.9: a) Correlation coefficients (shaded) between major hurricane CFAN wind field reconstructions and H*Wind analyses in radius of maximum winds relative distances. The stippling denotes where correlations are not statistically significant. b) Similar to a), expect for mean bias in kts (shaded). Positive biases indicate CFAN wind values are larger than H*Wind. c) Similar to a) and b), except for RMSE in kts (shaded). White concentric circles show RMW relative distances at normalized intervals of 0.25, 0.5, 0.75, 1, 1.5, and 2.

The model is able to explain more of the variance outside of 0.5 RMW for HUR and MHUR wind fields than NON wind fields, which may be expected since parametric models typically perform better for a well defined stronger system than a weaker TC. The magnitude of the biases and errors of the NON wind fields are lower than HUR and MHUR magnitudes. The amplified error near the eyewall for HUR and MHUR is likely a result of locally strong gradients in wind speeds, which would introduce uncertainty in the b parameter in H10. The larger errors in the surface winds near the inner circulation appear to have minor impact on the outer circulation.

In the NON wind fields the large area of low correlation coefficient near the center of circulation to 0.75 RMW suggest that the current methodology may not appreciate enough of the storm-relative asymmetries that often accompany a weak TC. These asymmetries may be a result of deep layer VWS or landfalling effects. Large errors occur inland after hurricanes make landfall and become weak, so land issues can cause asymmetries. VWS in the core region of a TC can have strong effects on the asymmetric structure of the eyewall region as well (Corborsiero and Molinari 2003).

To determine if VWS is a factor the CFAN algorithm should consider in its reconstructions, the wind fields were separated into low and high shear cases with the same analyses applied as above. Figure 3.10a shows the correlation coefficient for the low shear wind fields, which exhibited an average total variance outside 0.5 RMW explained of 95%. Figure 3.10b shows the correlation coefficient for the high shear wind fields, which explains an average total variance outside 0.5 RMW of 94%. The mean bias for the low shear cases is shown in Figure 3.11a, and the mean bias for high shear wind fields is shown in Figure 3.11b. The max mean bias at the RMW for both shear cases is

3.5 kts with a very similar average RMSE at the RMW (5.4 kts-low and 5.7 kts-high), as well (Figure 3.12a and b).

To further assess the possible shear limitation, the average radius of the 10kt RMSE was determined for each case. The low shear average 10 kt RMSE radius was 0.5953 RMW relative distance, and the high shear average 10 kt RMSE relative distance radius was 0.6197, which is a 0.0244 difference in RMW relative distance. As most of these qualities are similar and the structure of the errors between each case is alike, wind shear does not appear to be a major factor to explain the wind field asymmetry. However, two important aspects were not considered in this wind shear analysis. Cases with close proximity to landfall were not removed from the data set and a temporal requirement for the shear was not considered, which causes the analysis to assume the transition of the vortex from a symmetric to asymmetric system occurs instantaneously. A TC requires time to react to the shear's effect, creating the asymmetry.

a) b)

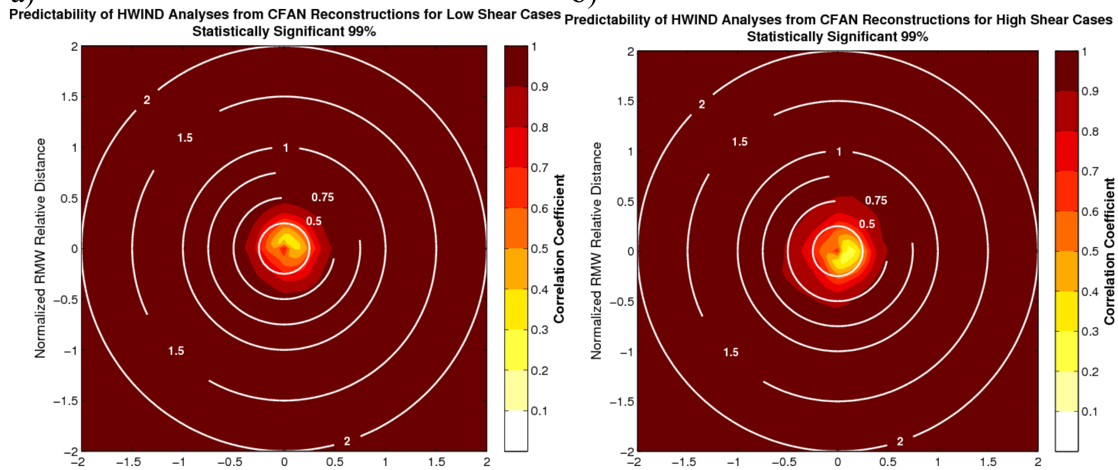

Figure 3.10: a) Correlation coefficients (shaded) between low shear CFAN wind field reconstructions and H*Wind analyses in radius of maximum winds relative distances. b) Similar to a) except high shear wind field reconstructions.

a) b)

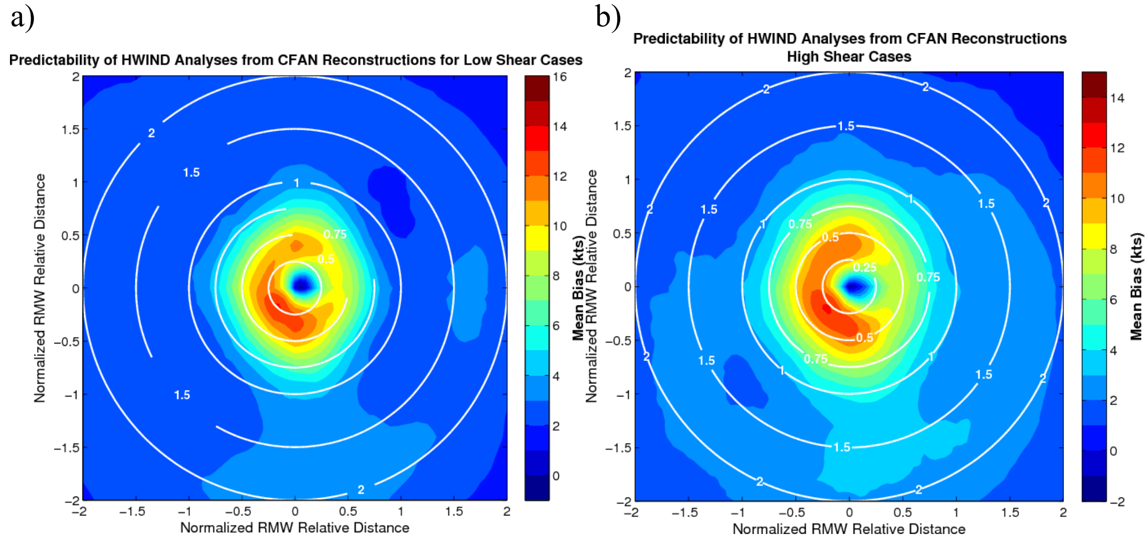

Figure 3.11: a) Mean bias (in kts; shaded) between low shear CFAN wind field reconstructions and H*Wind analyses in radius of maximum winds relative distances. b) Similar to a) except high shear wind field reconstructions.

a)

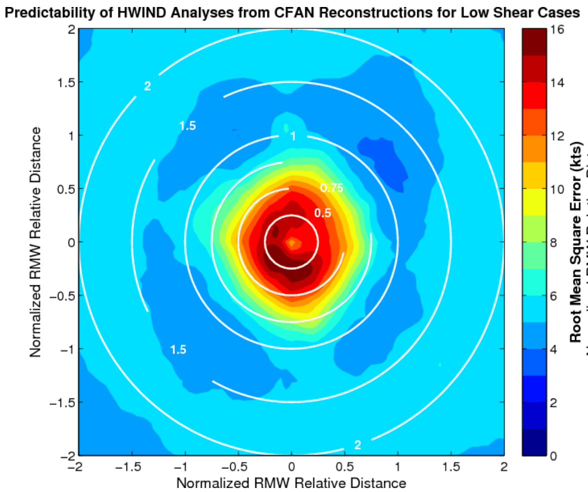

b)

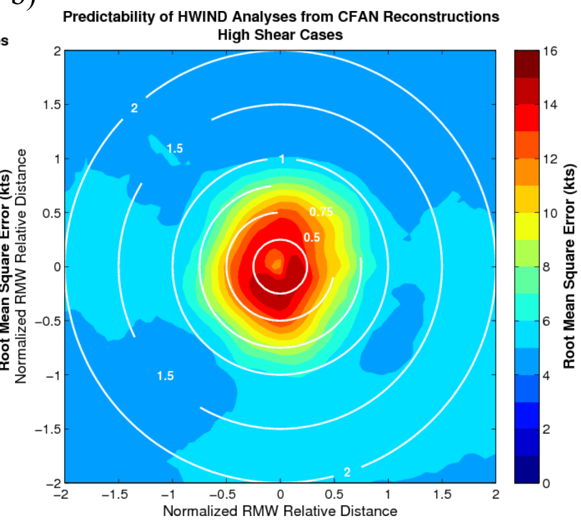

Figure 3.12: a) RMSE (in kts; shaded) between low shear CFAN wind field reconstructions and H*Wind analyses in radius of maximum winds relative distances. b) Similar to a) except high shear wind field reconstructions.

CHAPTER 4

CONCLUSION

Accurately forecasting the surface wind distribution in terms of structure and intensity for tropical cyclones is essential to anticipating potential coastal and inland hazards and for developing more effective evacuation strategies. This study has analyzed the CFAN surface wind field model, which is designed to generate high-resolution 2D surface winds for a tropical cyclones via a small set of wind radii information using the Holland et al. (2010) parametric wind model. The CFAN wind fields were evaluated against the H*Wind surface wind analyses to determine how well the CFAN model reproduces the surface winds in a tropical cyclone and to identify potential limiting factors that may be affecting the model's performance. This task was completed by comparing the CFAN and H*Wind model using the correlation coefficient, mean bias and RMSE. A total of 1584 surface wind cases from 2004–2012 were considered. The analysis considered how well the methodology reproduces the H*Wind analyses by conducting sensitivity analysis using varying resolution of initial input wind information, tropical cyclone type (NON, HUR and MHUR), and by the magnitude of vertical wind shear a TC experienced. Producing reconstructions with varying resolution of initial input wind information allowed for determining the minimum input wind resolution that is necessary to resolve on average the surface winds in a TC.

Results revealed that the CFAN surface wind field reproduction model explained most of the variability in the H*Wind wind fields meaning that it does an excellent job at reproducing TC wind fields outside of the center of circulation. The low variance within

0.25 RMW relative distances for all cases is consistent with the model treating the center of circulation as a point, whereas the center has a small, but finite lateral extent. For the resolution cases, 0.05° and 0.125° resolution input wind data was determined to be very suitable for generating correct high-resolution surface winds, and 0.25° input wind resolution data may utilized if a simple mean bias adjustment is also incorporated. The wind fields generated from 0.5° and 1.0° initial wind information did not perform well enough to be considered useful for accurate high-resolution TC wind field reproduction. This result means that if global model data is used to generate high-resolution wind fields, then the GFS and GEFS will need to be upgraded to finer spatial resolution before the CFAN wind field algorithm can be used to generate surface winds with high fidelity. Until these models are upgraded to finer resolution, one potential approach to generate reconstructions of the TC surface wind fields from these models would be to use other data sources for the location of the RMW and maximum winds, while using the coarse resolution data solely for the location of outer-wind radii.

As with most parametric models, the CFAN algorithm performed better for stronger TCs (HUR and MHUR) than weak TCs (NON) due to stronger systems being more well defined and usually more symmetric. The errors that were seen in the HUR and MHUR cases were likely a result of locally strong gradients near the eyewall that influence the b parameter in H10. The asymmetry in the NON cases could have been a result of several issues including: landfall, whereby the wind field gradually broadens after a TC moves inland, wind shear-induced asymmetries, or other environmental influences. In this analysis, one of these factors was considered by conducting a comparison of the surface wind distribution for low and high wind shear cases. However, the surface wind comparison conditioned on wind shear revealed that shear might not be a major limiting factor after all, although future work should remove the potential impact of landfall from this analysis and a temporal requirement should be included where the high shear must last at least 24 hours. In summary, the CFAN wind model is capable of generating high-resolution TC wind fields with high fidelity if initial wind field information is available at least at 0.25^{o} and for all storm types (except for asymmetries in NON cases).

The study did not cover the full scope of possible predictability limiting factors, so these issues need to continue to be analyzed. For the possibility of landfalling issues, wind fields where land occurs within 1 RMW from the center should be eliminated. It might be beneficial to also further break down the low and high shear cases by storm type as well, since this study only considered wind shear impacts across all storm types. Other limiting factors that should be assessed are the forecasts of the RMW, outer-wind radii, max intensity and track.

REFERENCES

Corbosiero, K. L., J. Molinari, 2002: The effects of vertical wind shear on the distribution of convection in tropical cyclones. *Mon. Wea. Rev*., **130**, 2110-2123.

Corbosiero, K. L., J. Molinari, 2003: The relationship between storm motion, vertical wind shear, and convective asymmetries in tropical cyclones. *J. Atmos. Sci*., **60**, 336-376.

Davis, C. W. Wang, J. Dudhia, and R. Torn, 2010: Does increased horizontal resolution improve hurricane forecasts?. *Wea. Forecasting*, **25**, 1826-1841.

DeMaria, Mark, Charles R. Sampson, John A. Knaff, Kate D. Musgrave, 2014: Is Tropical Cyclone Intensity Guidance Improving?. *Bull. Amer. Meteor. Soc.*, **95**, 387–398.

Done, J., C. Davis, and M. Weisman, 2004: The next generation NWP: Explicit forecasts of convection using the Weather Research and Forecast (WRF) model. *Atmos. Sci. Lett*., **5**, 110-117.

Fierro, A.O., R.F. Rogers, F.D. Marks, and D.S. Nolan, 2009: The impact of horizontal grid spacing on the microphysical and kinematic structures of string tropical cyclones simulated with the WRF-ARW model. *Mon. Wea. Rev*., **137**, 3717-3743.

Frank, W.M., and E.A. Ritchie, 2001: Effects of vertical wind shear on the intensity and structure of numerically simulated hurricanes. *Mon. Wea. Rev*., **129**, 2249-2269.

Gall, Robert, James Franklin, Frank Marks, Edward N. Rappaport, Frederick Toepfer, 2013: The Hurricane Forecast Improvement Project. *Bull. Amer. Meteor. Soc.*, **94**, 329–343.

Holland, G.J., J.I. Belanger, A. Fritz, 2010: A revised model for radial profiles of hurricane winds. *Mon. Wea. Rev*., **138**, 4393-4401.

Kain, J.S., S.J. Weiss, J.J. Levit, M.E. Baldwin, and P.R. Bright, 2006: Examination of convection-allowing configurations of the WRF model for the prediction of severe convective weather. The SPC/NSSL Spring Program 2004. *Wea. Forecasting*., **21**, 167-181.

Knaff, J.A., M. DeMaria, D.A. Molenar, C.R. Sampson, and M.G. Seybold, 2011: An automated, objective, multiple-satellite-platform tropical cyclone surface wind analysis. *J. Appl. Meteor. Climatol*., **50**, 2149-2166.

Leslie, L.M., R.F. Abbey Jr., and G.J. Holland, 1998: Tropical cyclone track predictability. *Meteorol. Atmos. Phys*., **65**, 223-231.

Neumann, C.J., B.R. Jarvinan, C.J. McAdie, and G.R. Hammer (1999), *Tropical Cyclones of the North Atlantic Ocean*, 1871-1998,206 pp., NOAA, Silver Spring, MD.

Plu, M., 2011: A new assessment of the predictability of tropical cyclone tracks. *Mon. Wea. Rev*., **139**, 3600-2608.

Saha, S., and Coauthors, 2012: The NCEP climate forecast system reanalysis. *Bull. Amer. Meteor.,* Soc., **91**, 1015-1057.

Schwartz, C.S. and Coauthors, 2009: Next-day convection allowing WRF model guidance: A second look at 2 km versus 4 km grid spacing. *Mon. Wea. Rev*., **137**, 3351-3372.

Vickery, P.J., D. Wadhera, M.D. Powell, Y. Chen, 2009: A hurricane boundary layer and wind field model for use in engineering applications. *J. Appl. Meteor. Climatol.,* **48**, 381-405.

Weisman, M.L., C.A. Davis, W. Wang, and K. Manning, 2008: Experiences with 0-36 h explicit convective forecasts with the WRF-ARW model. *Wea. Forecasting*., **23**, 407-437.

Zhang, F. and J.A. Sippel, 2009: Effects of moist convection on hurricane predictability. *J. Atmos. Sci*., **66**, 1944-1961.

Zhang, F. and D. Tao, 2013: Effects of vertical wind shear on the predictability of tropical cyclones. *J. Atmos. Sci*., **70**, 975-983.